Plant Soil (2025) 514:1263–1283
https://doi.org/10.1007/s11104-025-07462-y

RESEARCH ARTICLE

Novel polymeric nanoparticles as nanofertilisers for alkaline iron-deficient conditions

Simão Pinho · Carla Santos · Tânia Moniz · Andreia Granja · Mafalda Sarraguça · Salette Reis · Maria Rangel · Marta Vasconcelos

Received: 27 January 2025 / Accepted: 9 April 2025 / Published online: 30 April 2025
© The Author(s) 2025

Abstract

Background and aims Iron deficiency chlorosis (IDC) is a nutritional disorder impacting plants and is prevalent in calcareous alkaline soils, corresponding to 30% of the world's arable land. IDC compromises iron uptake in crops such as soybean (*Glycine max*). To improve the effect of iron fertilisers, we sought to develop a nanotechnology-based intervention using polymeric nanoparticles (NPs) loaded with $Fe(dmpp)_3$.

Methods Nanoparticles were loaded with a fluorophore to understand their uptake by soybean. Nanoparticles' physicochemical and release properties were examined. The work comprises a seed soaking study considering untreated plants, and $Fe(dmpp)_3$ solutions or nanosuspensions (NSs) (10 and 20 µM).

Results Plants treated with 20 µM NS showed an improvement in morpho-physiological traits and an increase in relevant gene expression *vs* control. They reached V1 stage 2.5 days faster and V3 2.8 days faster; had a 26% higher SPAD values at stage V3; developed roots that had 39% higher total fresh weight and shoots that were 26% heavier; and registered a 2.25-fold increase in root *IRT1* expression and a 3.37-fold increase in leaf *ferritin* expression. Treatment with 10 µM NS led to a 3.31-fold increase in *ferritin* expression *vs* control and a 2.49-fold increase *vs* $Fe(dmpp)_3$ solution at 10 µM.

Conclusions The results illustrate the potential of NPs as a seed-soaking agent, promoting plant growth, reducing IDC, and activating molecular-level iron

Responsible Editor: Stefano Cesco.

Supplementary Information The online version contains supplementary material available at https://doi.org/10.1007/s11104-025-07462-y.

S. Pinho · C. Santos · M. Vasconcelos (✉)
Universidade Católica Portuguesa, CBQF – Centro de Biotecnologia e Química Fina – Laboratório Associado, Escola Superior de Biotecnologia, Rua Arquiteto Lobão Vital 172, 4200 - 374 Porto, Portugal
e-mail: mvasconcelos@ucp.pt

S. Pinho · T. Moniz (✉) · A. Granja · M. Sarraguça · S. Reis
LAQV, REQUIMTE, Departamento de Ciências Químicas, Faculdade de Farmácia, Universidade Do Porto, Rua de Jorge Viterbo Ferreira, 228, 4050 - 313 Porto, Portugal
e-mail: tmoniz@icbas.up.pt

T. Moniz · M. Rangel
LAQV, REQUIMTE, Instituto de Ciências Biomédicas de Abel Salazar, Universidade Do Porto, Rua de Jorge Viterbo Ferreira, 228, 4050 - 313 Porto, Portugal

T. Moniz
LAQV, REQUIMTE, Departamento de Química E Bioquímica, Faculdade de Ciências, Universidade Do Porto, Rua Do Campo Alegre, S/N, 40160 - 007 Porto, Portugal

availability responses. Notably, this is the first study attempting to monitor the mobility of fluorescent NPs in soybean plants and the first in employing NPs as nanocarriers of $Fe(dmpp)_3$.

Keywords 3-hydroxy- 4-pyridinone · Iron deficiency chlorosis · Iron (III) chelate · Nanoparticle · Nanofertiliser · Rhodamine B

Introduction

Iron (Fe) is vital for the survival, growth and reproduction of all plants (Kobayashi and Nishizawa 2012). Due to its importance as a constituent of various proteins, iron plays a crucial role in biological processes such as respiration, nitrogen fixation, photosynthesis and DNA synthesis, in addition to serving as an active cofactor for numerous enzymes involved in plant hormone synthesis. (Rout and Sahoo 2015).

Despite the large supply of this mineral in most soils, its solubility in aerobic conditions is compromised by high-pH and calcareous soils (Kobayashi and Nishizawa 2012). This happens because in these conditions, iron tends to be oxidised to the ferric state (Fe^{3+}), after which it is likely bound to anions and other soil particles. This makes it harder for most dicotyledonous plants to uptake and transport it, since these plants rely on a membrane-bound ferric reductase to reduce iron to its more soluble ferrous state (Fe^{2+}), and this enzyme's action is restrained by high-pH (Marschner and Römheld 1994; Merry et al. 2022; Santos et al. 2021). Additionally, calcareous soils contain a large quantity of calcium carbonate, which, in conditions of high moisture, is dissolved, forming a solution containing calcium (Ca^{2+}) and carbonate (CO_3^{2-}) ions, the second being able to further increase the pH of soils, oxidizing Fe^{2+} to Fe^{3+}, as well as acting as a buffer, preventing dicotyledonous plants from lowering the soils' pH (Merry et al. 2022).

When iron is limited, such as in the case of alkaline soils, crops may develop iron deficiency chlorosis (IDC), which hampers crop productivity and negatively impacts the iron nutritional value of both vegetative states and edible plant parts. This condition is a significant nutritional disorder affecting plants growing on calcareous soils, usually with a pH ranging from 7.4 to 8.5, which decreases the availability of iron in the rhizosphere, impairing the plants' ability to uptake, transport and utilize this element (Lucena and Hernandez-Apaolaza 2017). In contrast, in soils with lower pH, iron remains more soluble and readily available, preventing these limitations (Morrissey and Guerinot 2009). This condition causes yellowing on the upper leaves, interveinal chlorosis and stunted growth, leading to a decline in yield and quality of a large number of crops, since around 30% of the world's total arable land is composed of calcareous soils, which in turn causes extensive monetary losses (Lucena and Hernandez-Apaolaza 2017; Santos et al. 2016a). For example, in the case of soybean (*Glycine max)* cultivation in the United States of America, IDC causes yearly yield losses of around 260 million US$ (Merry et al. 2022; Peiffer et al. 2012).

The application of different types of iron-based fertilisers is a regularly used method to reduce the effects of IDC and maintain high yields, consisting of ligands with an appropriate affinity for iron, high solubility in water and bioavailability (Carvalho and Vasconcelos 2013; Santos et al. 2016a). The main three types of iron fertilisers are: inorganic iron compounds, which are relatively inefficient in the soils, since they turn into insoluble compounds, being usually applied as foliar fertilisers; natural iron complexes, which are also quite unstable in the soil and usually applied in the same manner; and synthetic iron chelates, which possess certain artificial ligands that give them the desired properties for either foliar or soil application (Santos et al. 2016b). Another popular method for delivering fertilisers and biostimulants in plants is to conduct seed coating, in which seeds are enriched with the chosen nutrients and fertilisers before being sown (Skrzypczak et al. 2021).

Several iron (III) chelates derived from ligands such as ethylenediamine tetraacetic acid (EDTA) and ethylenediamine-*N,N*'-bis(o-hydroxyphenylacetic) acid (EDDHA) have been used in the soil as a way to provide the necessary supply of bioavailable iron. However, as many other commercial fertilisers, these compounds are extremely resistant to biodegradation, and can cause damage to the environment by binding to other heavy metals and potentially leaking to groundwater (Shinta et al. 2021; Ylivainio 2010). More recently, Fe chelates of 3-hydroxy-4-pyridinones (3,4-HPO), such as $Fe(mpp)_3$, $Fe(dmpp)_3$ and $Fe(etpp)_3$, have been demonstrated to enhance iron bioavailability in soybean plants, along with

improving the uptake of other minerals, increasing chlorophyll content, biomass production, and upregulating the expression of the *ferritin* gene, which encodes the primary protein responsible for iron storage. The latter Fe chelates also reduce the expression of the *IRT1* and *FRO2* genes, typically activated under iron deficiency stress, while exhibiting minimal toxicity (Santos et al. 2021).

This class of chelators has numerous potential advantages when compared to most fertilisers in the market, and $Fe(mpp)_3$, $Fe(dmpp)_3$ (herein called FeDM) and $Fe(etpp)_3$ have shown to deliver Fe^{3+} to hydroponically grown soybean plants successfully, and even prevent or mitigate some effects of IDC, with no observable negative side effects to the environment (Mesquita et al. 2020, 2022; Santos et al. 2022). However, as with other fertilisers, new strategies need to be put in place in order to reduce the amount of product that remains in the soil which may be achieved by employing different methods of application that provide a controlled uptake by the plants' roots.

One of the main issues with the current method of application of chemical fertilisers is that a considerable portion of these materials is not absorbed by crops, remaining on the soil instead, where they may eventually be leached, either horizontally or vertically to the groundwaters, or go into the atmosphere by volatilization (Vega-Vasquez et al. 2020). By utilizing nanocarriers such as nanoparticles (NPs) for the delivery of fertilisers, the uptake and interaction of nutrients can be augmented, improving release profiles, enhancing uptake efficiency and increasing yields, therefore offering relevant environmental and economic advantages (Mastronardi et al. 2015; Mittal et al. 2020). This efficiency is exacerbated by the fact that plant roots, as well as leaves, are extremely porous on the nano level, allowing for NPs to enter the plant more easily, either via root or foliar application (Mastronardi et al. 2015). While there are some concerns about the safety of the usage of NPs in the soil, certain types of polymeric NPs, such as PLGA-based NPs, have been widely used in the medical industry due to their biodegradability, biocompatibility and non-toxicity, and have been authorized by both EMA (European Medicines Agency) and the FDA (Food and Drug Administration) for varied therapeutic applications (Hua et al. 2021; Khodakovskaya and Marmiroli 2023). Despite this, PLGA's possible toxic effects on soil have to be thoroughly studied in order to guarantee its safety as a polymeric nanocarrier.

Thus, the main goal of this study was to develop polymeric NPs capable of delivering an iron chelate of the 3,4-HPO class, FeDM, to soybean plants grown under alkaline, iron-deficient conditions. To our knowledge, this is the first study exploring the potential of polymeric NPs with these chelates, contributing to the management of IDC.

Fluorescently labelled NPs with rhodamine B (RB) were prepared to investigate the uptake of NPs by plant roots. Different-sized polymeric NPs were designed, and their morphological and release properties were analysed. These labelled NPs were then evaluated for root uptake and then plants' tissues were analysed by confocal fluorescence microscopy, with the objective of determining the most suitable NP size for future development of iron nanofertilisers. Subsequently, the study continued to produce iron nanofertilisers by replacing the RB labelling with the iron chelate FeDM. The NPs were then characterized for their morphological and release properties, and their stability over time was assessed. Finally, the effectiveness of these nanofertilisers on plants grown under iron-deficient conditions was assessed through both morphological and genetic analysis, focusing on the expression of the root *FRO2* and *IRT1* genes, as well as the leaf *ferritin* gene.

Materials & methods

Synthesis and characterization of Fe-chelates

The 3,4-HPO ligand Hdmpp was acquired from (Sigma-Aldrich®, St. Louis, MO, USA). Its corresponding Fe(III) chelate, FeDM, was prepared in our laboratory following previously described procedures (Queiros et al. 2011; Schlindwein et al. 2006). Chelate was characterized by Elemental analyses (EA) (C, H, N) at the analytical services of University of Santiago (Spain). The EA results for the Fe(III) chelate revealed that the complex was obtained as a hydrate and is consistent with the formulae: $[Fe(dmpp)_3]0.3H_2O$. Elemental analysis for $C_{21}H_{24}N_3O_6Fe.3H_2O$, % calculated (% Found): C 48.11 (48.17) H 5.77 (5.34) N 8.01 (7.88).

Preparation of rhodamine B-loaded nanoparticles

To obtain several different-sized NPs, several strategies for their production were considered, with the objective of selecting three distinct types of formulations, which were labelled as "small", "medium" and "large" nanosuspensions (NSs), according to the size of their NPs. Firstly, a rhodamine B (RB) (Sigma-Aldrich®, St. Louis, MO, USA) stock solution (1 $mg.mL^{-1}$) was prepared, by dissolving RB in acetone (VWR Chemicals, Radnor, PA, USA) and using an ultrasonic bath to homogenize the mixture.

The NS labelled as "small" was created by nanoprecipitation. Firstly, 10 mg of PLGA (Corbion® PDLG 5004 A, Amsterdam, Netherlands) were dissolved in 650 µL of acetone and 150 µL of 99% ethanol (Labchem®, Zelienople, PA, USA) as well as 200 µL of the previously described RB solution. This solution was then injected quickly by syringe to 10 mL of double-deionized water (Arium Pro, Sartorius AG, Gottingen, Germany; 18.2 MΩ.cm resistivity) with vigorous stirring and at 20 ºC and left in those conditions for 3 h, after which it was filtered using a 200 nm filter. After this, the suspension was left at 4ºC for 24 h (Chang et al. 2009).

Additionally, another NS labelled as "medium" was prepared by dissolving 10 mg of PLGA in an organic phase of 100 µL RB solution and 900 µL acetone and slowly adding everything to a 5 mL solution of 0.1% PVA (Sigma-Aldrich®, St. Louis, MO, USA) in deionized water. The resulting solution was then sonicated for 1 min at 70% using a VCX-130 Vibra-Cell™ Ultrasonic Liquid Processor sonicator (Sonics & Materials®, Newtown, CT, USA). The samples were then added to 5 mL of 0.1% PVA solution and left stirring in a heating place (IKA Werke®, Staufen, Germany) at medium speed and 20 ºC overnight, after which it was placed at 4ºC for 24 h (Chaves et al. 2018).

Finally, the NS labelled as "large" was prepared by dissolving 8 mg of PLGA in 1 mL of dichloromethane (Honeywell®, Charlotte, NC, USA) and 30 µL of RB stock solution. This organic phase was then added to 2 mL of a 2% PVA solution, after which the resulting solution was sonicated at 70% intensity for 30 s and placed in a heating plate with high speed stirring and 20 ºC for 3 h (Fonseca et al. 2021).

For the three types of RB-loaded NPs (RB-NPs), the respective NSs of unloaded NPs were prepared for comparison, by using the same strategies employed in the formulations of RB-NPs but replacing the volume of RB stock solution by the same amount of the organic solvent used in each strategy.

Physicochemical characterization of rhodamine B-loaded nanoparticles

To analyse the NPs' size, polydispersity index (PDI) and zeta potential, the Dynamic Light Scattering (DLS) device ZetaPALS (Brookhaven Instrument Corps, Holtsville, NY, USA) was used. Both mean particle size and PDI were obtained by using a light incidence angle of 90º at 25 ºC, and the obtained results were the mean of a total of four runs of 2 min. The zeta potential was analysed at 20 ºC, with a total of eight runs of ten cycles each. The same studies were performed for unloaded NPs.

All prepared NPs, as well as all the reagents used for their preparation, were also characterized by Fourier-transform infrared spectroscopy (FTIR) analysis, using Frontier FT-IR spectrophotometer (PerkinElmer, Beaconsfield, UK) equipped with an attenuated total reflectance (ATR) accessory. Spectra were collected in the wavenumber range of 4000–600 cm^{-1}, with 32 scans per sample and a resolution of 4 cm^{-1}.

To analyse the encapsulation efficiency (EE) and loading capacity (LC) of the produced NPs, a calibration curve of RB fluorescence in water was performed and analysed in a Synergy™ HT plate reader (Biotek®, Winooski, VT, USA). Several dilutions were therefore prepared, using a 0.5 $mg.mL^{-1}$ RB solution in 10% ethanol, and then had their fluorescence analysed at the excitation wavelength of 485 nm and emission wavelength of 495 with a gain of 50%. Successive dilutions were made to obtain the following standards (4.7, 9.4, 18.8, 37.5 and 75 $mg.mL^{-1}$) and the linear correlation defined by the equation $y = 899424x\text{-}167{,}59$, $R^2 = 0{,}9996$. The calibration curve was performed in triplicate.

Then, NS samples (2 mL) were centrifuged at 11000 rpm and 20ºC for 30 min. Then, 200 µL of supernatant was transferred to a microplate and its absorbance was analysed considering the previously described conditions used for the calibration curve.

The EE represents the percentage of compound incorporated into the polymeric matrix of the NPs compared to the total amount of the same compound

used for the encapsulation process (Giridhar Reddy and Thakur 2019). It is calculated using the following formula:

$$\%EE = \frac{total\ compound\ mass - free\ compound\ mass}{total\ compound\ mass}$$

The LC is defined as the total mass of the compound incorporated into the polymeric matrix divided by the mass of the total polymeric system (Massella et al. 2018). It is calculated using the following formula:

$$\%LC = \frac{total\ compound\ mass - free\ compound\ mass}{total\ compound\ mass + total\ polymer\ mass}$$

A release study was also performed for RB NSs, in which 500 µL of each NS was mixed with 1.5 mL of deionized water in microtubes and incubated at 25ºC and 50 rpm. This process was repeated several times for each one, since the incubation periods evaluated were 0 min, 15 min, 30 min, 45 min, 1 h, 2 h, 4 h, 5 h, 6 h, 1 day, 2 days and 3 days in triplicates. After the incubation time, the tubes were centrifuged at 11000 rpm for 30 min and at 20 ºC. After this, 200 µL of the supernatant of each tube was transferred to a microplate and analysed in the same conditions as mentioned before, in order to determine the amount of RB released by each NP over time.

Evaluation of nanoparticle uptake by soybean plants

Soybean seeds were germinated in wet filter paper on Petri dishes and left in the dark at room temperature for a week.

After germination, ten seeds were transferred to a hydroponic system. A nutrient solution was prepared according to (Santos et al. 2020). A ferric sodium solution (FeNaEDDHA) was prepared and added to each hydroponic growth pot independently for a final concentration of 40 µM. The pH of the solutions was monitored using an IKA RH basic 2 pH meter (IKA Werke®, Staufen, Germany) and buffered with a 200 mM (2-(N-morpholino)ethanesulfonic acid) (MES) medium solution (Sigma-Aldrich®, St. Louis, MO, USA) and regulated to 5.5.

Plants were grown in pots (5 dm^3) under hydroponic conditions and in a climate chamber (Aralab Fitoclima 10000EHF) maintained at a 16-h photoperiod, providing a photosynthetic photon flux density of 325 µmol m^{-2} s^{-1} at plant level, supplied by a combination of incandescent and fluorescent lights. During the light period, the temperature was kept at 25ºC, while during the dark period it was set to 20 °C, and relative humidity was maintained at 75% in both periods. The experiment continued for two weeks, in which the hydroponic solution, along with FeNaEDDHA, was renewed at the 7 th and 10 th days.

After the 14 th day, plants were carefully removed from their pots, and their respective roots were placed, in duplicate, in contact with 40 mL of different RB solutions/NSs for 24 h. These groups included the "small","medium" and "large" NSs, as well as a 20 µM aqueous RB solution, and a control group with deionized water.

After incubation, two samples of the main root, stem and first trifoliate leaves of each plant were cut, separated, and kept in formaldehyde (Merck, Darmstadt, Germany) for sectioning and preparation for analysis. Each sample was paraffin-embedded and sectioned at a thickness of 5 µm without any additional staining. Then, histological analysis was performed by fluorescence microscopy. Images were acquired with a resolution of 1024 × 1024 using a 10 × objective.

Each microscope slide, containing at least three sections of each replica from roots, stems and leaves, was analysed by a Leica Stellaris 8 confocal microscope (LeicaMicrosystems, Wetzlar, Germany) equipped with the Leica Application Suite X package (LAS X). The wavelength chosen was 560 nm for excitation and 575 nm for emission. The obtained images were processed using ImageJ software in order to get qualitative information on the uptake of the different RB NPs, along the different tissues of the plant. To quantify the mean fluorescent intensity (MFI) of each condition, at least three different regions of the two different microscope slides were captured and analysed using Fiji ImageJ.

Confocal microscopy assays were conducted at the Imaging by Confocal and Fluorescence Lifetime Laboratory, CEMUP (Centre of Materials of University of Porto), Portugal.

Preparation of iron chelate-loaded nanoparticles

Firstly, a stock solution of FeDM (10 $mg.mL^{-1}$) was prepared in methanol (VWR Chemicals, Radnor, PA, USA). The production of FeDM-loaded NPs (FeDM-NPs) was based on the formulations previously used

in the preparation of RB-NPs but using the FeDM stock solution instead of the RB stock solution.

Physicochemical characterization of iron chelate-loaded nanoparticles

The analysis of the NPs' size, PDI and zeta potential was performed as previously for the RB NSs. FTIR spectra were obtained to verify the encapsulation of the chelate in the formulation, following the same procedure used for RB-NPs.

To determine the encapsulation efficiency (EE) and loading capacity (LC) of the iron chelate NSs, a calibration curve of FeDM absorbance in water was created. Dilutions were made from the stock solution to obtain the following standards (0.007, 0.014, 0.021, 0.035, 0.042, 0.056 and 0.063 $mg.mL^{-1}$) and the linear correlation defined by the equation $y = 6{,}2166x + 0{,}0289$, $R^2 = 0{,}9999$. The calibration curve was performed in triplicate and the absorbance was determined at 455 nm.

For the EE and LC determinations, 2 mL of each NS was centrifuged at 11,000 rpm and 20ºC for 30 min. Then, 200 µL of supernatant was transferred to a microplate and analysed as described for the calibration curve.

A release study was also performed for FeDM NSs, which was executed with the same conditions and times as the one previously described for the RB NSs.

With the objective of determining the storage life of the FeDM-NPs both at room temperature (≈21ºC) and at 4ºC, stability studies were performed. At least three replicates of each NS type were prepared and stored along six weeks at both described temperatures. The analysis of particle's size, PDI, zeta potential, EE and LC was performed considering freshly prepared formulations and after 1, 2, 4 and 6 weeks of storage.

Study of the effect of FeDM-loaded nanoparticles in soybean plants

Seed coating and soil cultivation studies

To obtain a soil with an easily controlled pH, a standard artificial soil was created, containing, in relative mass, 70% quartz sand (Intex®, Portugal), 20% expanded clay (Argex®, Portugal) and 10% peat (Siro®, Portugal), according to the OECD standard protocol (OECD 1984; Santos et al. 2021). In order to increase the pH of the soil to simulate alkaline soils, 1 g of calcium oxide (CaO) (Tintinhas®, Portugal) was added for each kg of soil, in order to reach the pH of 8. The different components were then homogenized thoroughly.

Afterwards, solutions of the chelate FeDM at concentrations of 20 µM and 10 µM were prepared by diluting the FeDM stock solution in deionized water. These concentrations were chosen based on a previous study conducted in hydroponic conditions (Santos et al. 2020). The "medium" FeDM-NPs were selected for this study due to their favourable morphological, physicochemical, as well their similarity to the "medium" RB-NPs and the fact these were more successful in providing the encapsulate to plant leaves. These FeDM-NPs were also diluted to 20 µM and 10 µM in deionized water.

Plants were divided into five groups of five replicates each: four of the groups were treated with FeDM solutions (10 µM or 20 µM) or NSs at the same concentrations, while the control group received water; seeds were submerged in their respective treatments for 24 h in darkness at room temperature. After the coating process, each group of seeds was transferred to a petri dish, with moistened filter paper with the corresponding solution or suspension. The setup was then kept in the dark, at room temperature, for an additional 48 h.

The seeds were individually sown, one per pot (0.5 dm^3) with the previously described artificial soil, and plants were watered every two days with 80 mL of the nutritive solution described previously (without FeNaEDDHA). Plants were kept under a 16-h photoperiod, receiving 325 µmol m^{-2} s^{-1} of photosynthetic photon flux density at plant level, provided by a combination of incandescent and fluorescent lights. Temperatures were maintained at 25 ºC during the light period and at 20 ºC during the dark period, and relative humidity was kept at 75% throughout both periods. These conditions were maintained throughout the study, which lasted for three weeks from the sowing date.

Morphological and productivity parameters

Plant height was measured daily, and the dates of formation and maturation of each trifoliate were

recorded. Leaf chlorosis was assessed from developmental stages V1 (one fully expanded trifoliate leaf) to V3 (three fully expanded trifoliate leaves) with Leaf Soil–Plant Analysis Development (SPAD) readings, measured with a portable chlorophyll meter (Konica Minolta SPAD- 502Plus) using the latest trifoliate leaf of each individual replicate. The plants were maintained for three weeks starting from the sowing date until the V3 phenological stage was reached. At this stage, plant tissues were firstly separated between the root and the aerial part, to measure the root and shoot fresh weight. The samples were then stored at 80ºC.

Gene expression analysis

Plants' individual roots and V3 trifoliate leaves were pulverized in liquid nitrogen, and the total RNA was extracted using RNeasy® Plant Mini Kit (#74,904) (Qiagen, Hilde, Germany), as per the manufacturer's guidelines. The quantity and quality of the extracted RNA were verified using UV-spectrophotometry, using a nanophotometer (Implen, Isaza, Portugal). Posteriorly, single-strand cDNA was synthesized using the protocol and reagents provided by iScript™ cDNA Synthesis Kit (Bio-Rad, Laboratories, Inc, Hercules, CA, USA). *ferritin*, *FRO2* and *IRT1* primer sequences, as well as the ones for the reference genes *18S* and *ACTIN* were taken from (Santos et al. 2020), which also details the qPCR protocol followed in this study. The annealing temperature of each primer are shown in Table A.1. The relative quantification of iron-related genes' expression values was carried out using the comparative ΔΔCt method (Livak and Schmittgen 2001), where the geometric mean of the expression of the two reference genes (*18S* and *ACTIN*) is used as controls and the samples from plants not treated with iron as reference samples. Two technical replicates were analysed, and the data were exported to Excel files for visualization as graphs depicting the normalized fold expression of the target genes.

Structural analysis of plants' leaves by FTIR and PLSDA

To elucidate the structural impacts on plants' leaves treated with FeDM, FTIR analysis was performed on a subset of V3 trifoliates prepared for genetic analysis. Samples were analysed using a previously described FTIR instrument with 16 scans and an 8 cm^{-1} resolution. Pulverized leaves were placed in an ATR crystal under constant pressure, and spectra were collected in triplicate. Background spectra were acquired with an empty ATR accessory.

Partial least squares discriminant analysis (PLSDA) was employed to differentiate between control plants (class 1) and those treated with FeDM solutions (class 2) or NPs (class 3). Spectra were divided into four spectral regions:

- **R1:** 3000–2800 cm^{-1} (C-H stretching)
- **R2:** 1810–1484 cm^{-1} (C =O stretching, C–C stretching)
- **R3:** 1484–1188 cm^{-1} (C-H bending, C-O stretching)
- **R4:** 1188–882 cm^{-1} (C-O stretching, C–C stretching)

These spectral regions are indicative of specific chemical bonds and functional groups, offering insights into the structural alterations induced by FeDM treatments.

Five pre-processing techniques (SNV, Savitzky-Golay filtering with first and second derivatives, and their combinations) were evaluated. Spectra were randomly divided into 70% calibration and 30% validation sets, and PLSDA was performed 100 times with cross-validation. The optimal model was selected based on the highest overall prediction accuracy across latent variables (1 to 7), spectral regions, and pre-processing methods.

PLSDA analyses were performed using MATLAB 2022a software version R2022a Update 5 (9.12.0.2039608) (MathWorks, Natick, MA, USA) and PLS Toolbox version 9.2.1 (2023) (Eigenvector Research Inc., Manson, WA, USA).

Statistical analysis

Statistical analysis was performed using GraphPad Prism Software (Version 9.0 for Windows; GraphPad Software Inc, San Diego, CA, USA). T-student test, one-way and two-way ANOVA analysis of variance was used to assess the differences in the results. The statistical test used is specified in each case. All the

analysis were performed considering at least triplicates from each studied condition.

Results

Physiochemical Characterization of rhodamine B-loaded nanoparticles

The results obtained on the physiochemical and release properties of RB-NPs are represented on Table 1. Each property was compared between groups by one-way ANOVA with Tukey's multiple comparisons test. "Large" RB-NPs are significantly larger ($p < 0.005$) than the other two, and "medium" RB-NPs are significantly larger ($p < 0.001$) than "small" RB-NPs. Regarding zeta potential, the "small" RB-NPs have significantly lower values than the other two NPs ($p < 0.05$). Finally, "medium" RB-NPs have a significantly higher EE and LC than "small" and "large" RB-NPs ($p < 0.005$).

The three types of unloaded NPs produced based on the previous methods for the RB-NPs were then analysed, and their physicochemical properties were then compared to the ones of the RB-NPs of the same type with an unpaired t-test with Welch's correction, to determine the impact of the compound in the properties of the NPs, which is an indication of the expected load of RB into the NP matrix. The results obtained by the analysis of their physicochemical properties are shown in Table 1. When compared to the "small" RB-NPs, no statistically relevant differences were encountered related to size. The unloaded "medium" NPs are significantly smaller than the "medium" RB-NPs ($p < 0.05$). This enlargement may be due to the presence of the compound inside the particle, which was entrapped in a higher extension (large EE% found). Finally, no significant differences were found between "large" unloaded and RB-NPs.

The RB-NPs unloaded NPs and the reagents that compose them were also characterized by FTIR spectroscopy. The results are represented on Fig. 1.

In the high wavenumber region (Fig. 1 (a)), the characteristic OH stretching band of the alcohol group of PVA can be easily seen at 3310 cm^{-1}. Furthermore, the CH asymmetric stretching of PVA can be seen in this region at around 2930 cm^{-1} (Kharazmi et al. 2015). These bands are also present in "medium" and "large" NPs, which have PVA in their constitution. In the fingerprint region (Fig. 1 (b)), the characteristic peak of the carbonyl stretching at 1749 cm^{-1} can be seen in the spectrum of PLGA (Bukhari et al. 2023) and in all NPs produced since all of them have PLGA in their constitution. The incorporation of RB in the NP can only be seen for "small" RB-loaded NPs, as can be observed by the peaks at 1644, 1588, and 1338 cm^{-1}, bands corresponding to RB that are present in the "small" RB-NPs.

Afterwards, a study on the release profile of the previously described "small", "medium" and "large" NPs was conducted, to determine the ability of the formulations to retain or release RB.

From the data acquired, it is noticeable that for all three types of NPs, the amount of compound released remains stable over three days, at 25 ºC and 50 rpm, in water. These results show that all three NSs have the potential to keep a significant amount of RB encapsulated for that time. This data is represented in Figure A.1.

Table 1 Size, polydispersity index (PDI), zeta potential, encapsulation efficiency (EE) and loading capacity (LC) of "small", "medium" and "large" RB-NPs, as well as size, PDI and zeta potential of unloaded-NPs

	"Small" RB-NPs	"Medium" RB-NPs	"Large" RB-NPs	"Small" unloaded-NPs	"Medium" unloaded-NPs	"Large" unloaded-NPs
Size (nm)	121 ± 3^{a}	246 ± 6^{b}	322 ± 33^{c}	110 ± 6	220 ± 8^{d}	368 ± 64
PDI	0.09 ± 0.04^{a}	0.10 ± 0.03^{a}	0.15 ± 0.01^{a}	0.10 ± 0.01	0.07 ± 0.01	0.26 ± 0.06
Zeta Potential (mv)	-15 ± 5^{a}	-6.6 ± 0.2^{b}	-4.0 ± 1.3^{b}	-10.0 ± 2.6	-6.2 ± 0.3	-4.3 ± 1.1
Encapsulation Efficiency	31.3 ± 4.1	72.3 ± 5.6	38.5 ± 11.2			
Loading Capacity	0.63 ± 0.06	1.4 ± 0.10	0.17 ± 0.06			

[a,b c] indicate significant differences ($p < 0.05$) between RB-NPs by one-way ANOVA with Tukey's multiple comparisons test

[d] indicates significant differences ($p < 0.05$) between unloaded-NPs and RB-NPs by one-way ANOVA with unpaired t-test with Welch's correction

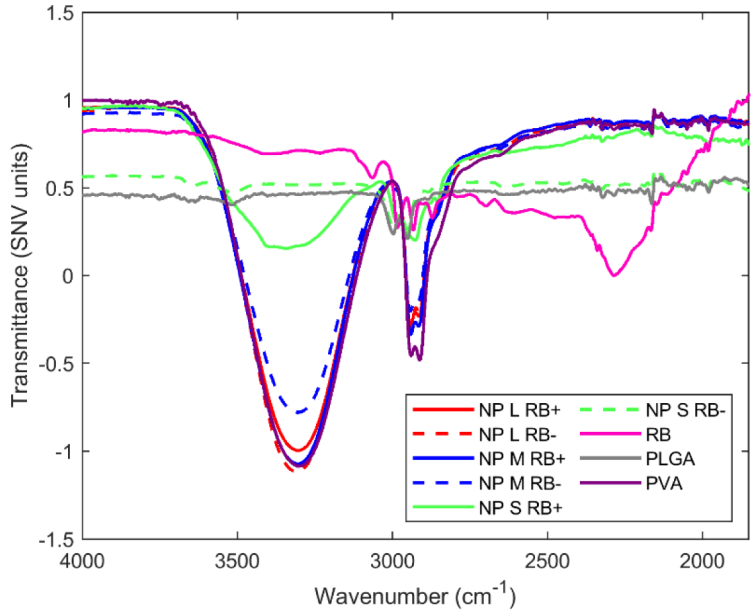

(a)

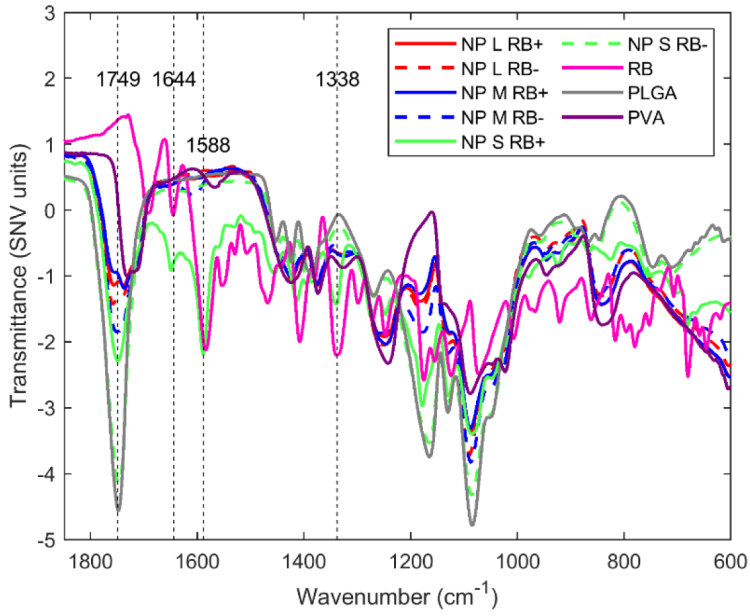

(b)

Fig. 1 Fourier-transform infrared spectroscopy spectra of the three types (L-Large; M-Medium; S-Small) of rhodamine B-loaded nanoparticles (RB+), their unloaded counterparts (RB-), Poly(D,L-lactide-co-glycolide) (PLGA), rhodamine B (RB) and Poly(vinyl alcohol) (PVA), from 4000 cm^{-1} to 1850 cm^{-1} **(a)** and from 1849 to 600 cm^{-1} **(b)**

Evaluation of rhodamine-B loaded nanoparticles' uptake by soybean plants

The first inspection on the uptake of RB-NPs by soybean plants grown was performed in hydroponic culture. After 14 days of growth, ten plants were divided in groups of two and placed in contact with NSs of "small", "medium", "large" RB-NPs, a 20 µM RB water-based solution, as well as deionized water (control). After 24 h, the roots (R), stems (S) and leaves (L) were collected and later analysed by confocal microscopy to determine which type of NPs are more efficiently taken up by the plants (Fig. 2). A quantitative analysis was also performed using Fiji ImageJ (Fig. 3), revealing that at the root level, plants treated with "medium" RB-NPs had a higher fluorescence intensity than plants treated with RB solution, "small" FeDM-NPs and control ($p < 0.05$), while the group treated with "small" RB-NPs exhibited more fluorescence than the one treated with RB solution and control ($p < 0.05$). The group exposed to "large" RB-NPs had more fluorescence intensity than the ones exposed to RB solution and control ($p < 0.05$). Regarding the stems, plants treated with "medium" RB-NPs demonstrated significantly more fluorescence intensity than all the other groups of plants ($p < 0.05$), while "small" and "large" RB-NPs, as well as RB solutions presented a more intense signal than control ($p < 0.05$). Finally, in the leaves, plants treated with "medium" RB-NPs had a higher fluorescence intensity than all other groups except the one treated with RB solution ($p < 0.05$), while "small" and "large" RB-NPs, as well as the RB solution, exhibited more signal than control ($p < 0.05$).

Production and characterization of iron chelate-loaded nanoparticles

The subsequent phase of the study involved developing NPs, similar to the ones developed in the previous sections, but loaded with the 3,4-HPO iron chelate FeDM, in order to later be assessed in vivo

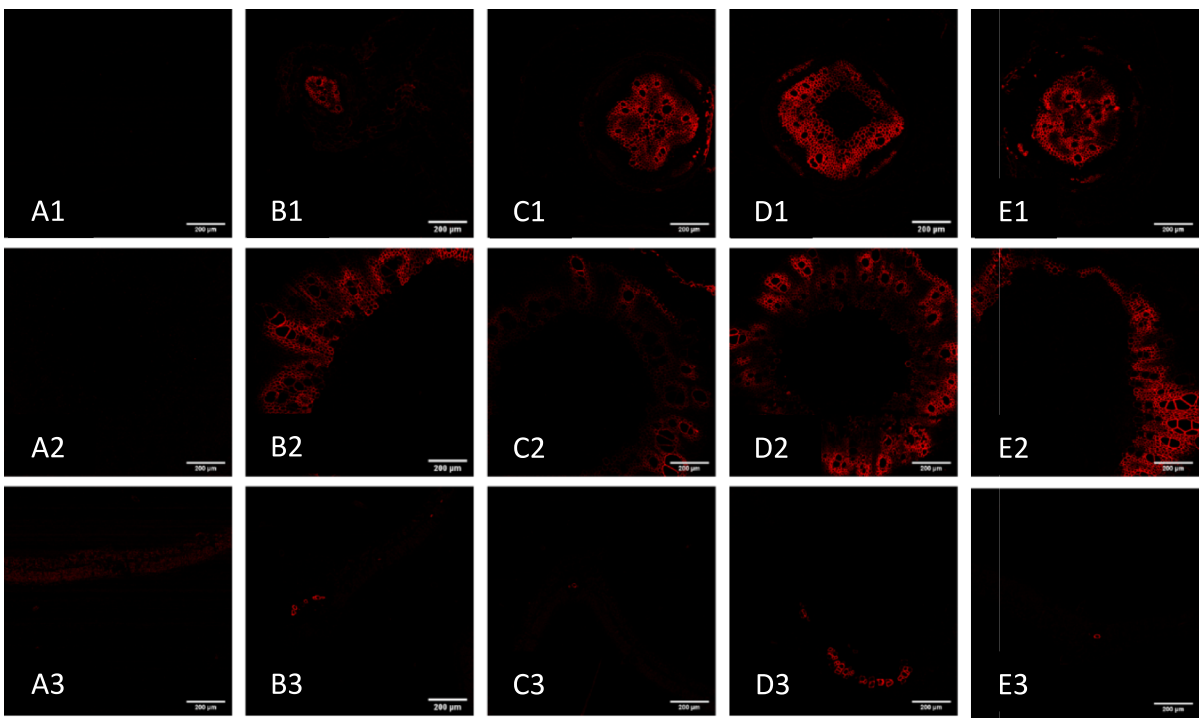

Fig. 2 Representative image of the detected fluorescence signals (represented as the colour red) at an excitation wavelength of 560 nm and an emission wavelength of 575 nm for each plant organ (1–3) under different treatments (A-E). (**A**) Control group, (**B**) Rhodamine B solution, (**C**) "small" RB-NPs, (**D**) "medium" RB-NPs (**E**) "large" RB-NPs. (1) Roots (R), (2) Stems (S), (3) Leaves (L)

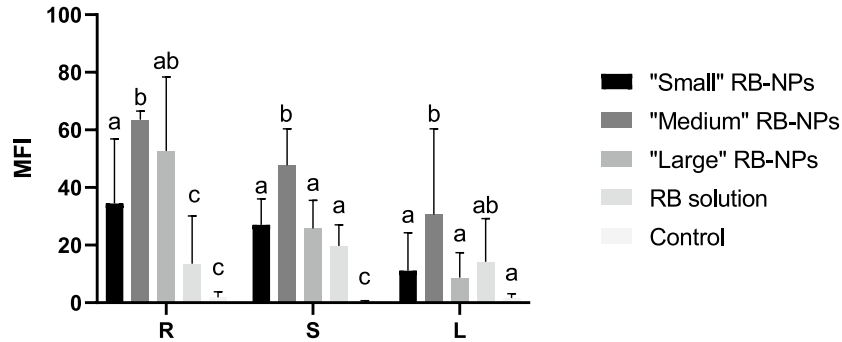

Fig. 3 Quantitative analysis of the mean fluorescence intensity (MFI) of each plant organ: Roots (R), Stems (S) and Leaves (L) under different treatments: "small" RB-NPs, "medium" RB-NPs, "large" RB-NPs, RB solution and control. At least 3 different regions from 2 different microscope slides were captured and data were analysed using Fiji ImageJ. Differences between treatments were assessed using two-way ANOVA followed by Tukey's test. Different letters in each plant organ indicate significant differences ($p < 0.05$)

in soybean plants. The three types of NPs are based on the protocols used for the RB NSs with the same designation. The results obtained from analysing their sizes, PDI, zeta potentials, EEs and LCs are depicted in Table 2. Data was analysed by one-way ANOVA with Tukey's multiple comparisons test. "Large" FeDM-NPs are significantly larger than both other types ($p < 0.005$), and "medium" FeDM-NPs are larger than "small" FeDM-NPs ($p < 0.05$). Relating to zeta potential, "medium" and "large" FeDM-NPs have significantly lower values than "small" FeDM-NPs ($p < 0.05$). Finally, "small" FeDM-NPs have a significantly higher LC than the other two types of NPs ($p < 0.05$).

The spectra in Fig. 4 (a), depict the presence of the PVA characteristic peak at 3310 cm^{-1} representing an OH stretching. In the same region, a peak is also seen in the spectrum of FeDM, although with a broader and weaker signal which may be assigned to the OH vibration group of the water contained in the chelate. This peak is seen in all NPs, due to the presence of FeDM. The sharp band at 1750 cm^{-1} is due to the carbonyl group of PLGA and can also be seen in all the NP. The incorporation pf the FeDM into the NPs can be proven by the bands at 1600 cm^{-1} and 1544 cm^{-1} from FeDM that are present in all the NPs produced.

A study on the release profile of the "small", "medium" and "large" FeDM-NPs was conducted, to determine the ability of the formulations to retain or release the chelate. Through the analysis of Fig. 5, it was determined that for all three types of NPs, the amount of compound released remains stable over three days, at 25 ºC and 50 rpm, in water. The released mass corresponds approximately to the unloaded amount of chelate determined for the freshly prepared NPs. These results show that all three NSs have the potential to keep a significant amount of the iron chelate encapsulated for that time.

Table 2 Size (**a**), polydispersity index (PDI) (**b**), zeta potential (**c**), encapsulation efficiency (EE) (**d**) and loading capacity (LC) (**e**) of "small", "medium" and "large" FeDM-NPs

	"Small" FeDM-NPs	"Medium" FeDM-NPs	"Large" FeDM-NPs
Size (nm)	97 ± 18^{a}	170 ± 18^{b}	287 ± 10^{c}
PDI	0.30 ± 0.04^{a}	0.18 ± 0.03^{a}	0.18 ± 0.02^{a}
Zeta Potential (mv)	-2.6 ± 0.7^{a}	-7.9 ± 0.5^{b}	-5.7 ± 0.4^{b}
EE (%)	31 ± 5^{a}	29 ± 2^{a}	38 ± 1^{a}
LC (%)	5.2 ± 0.8^{a}	2.6 ± 0.1^{b}	1.3 ± 0.3^{b}

^{a,b} indicate significant differences ($p < 0.05$) between groups of FeDM-NPs by one-way ANOVA with unpaired t-test with Welch's correction

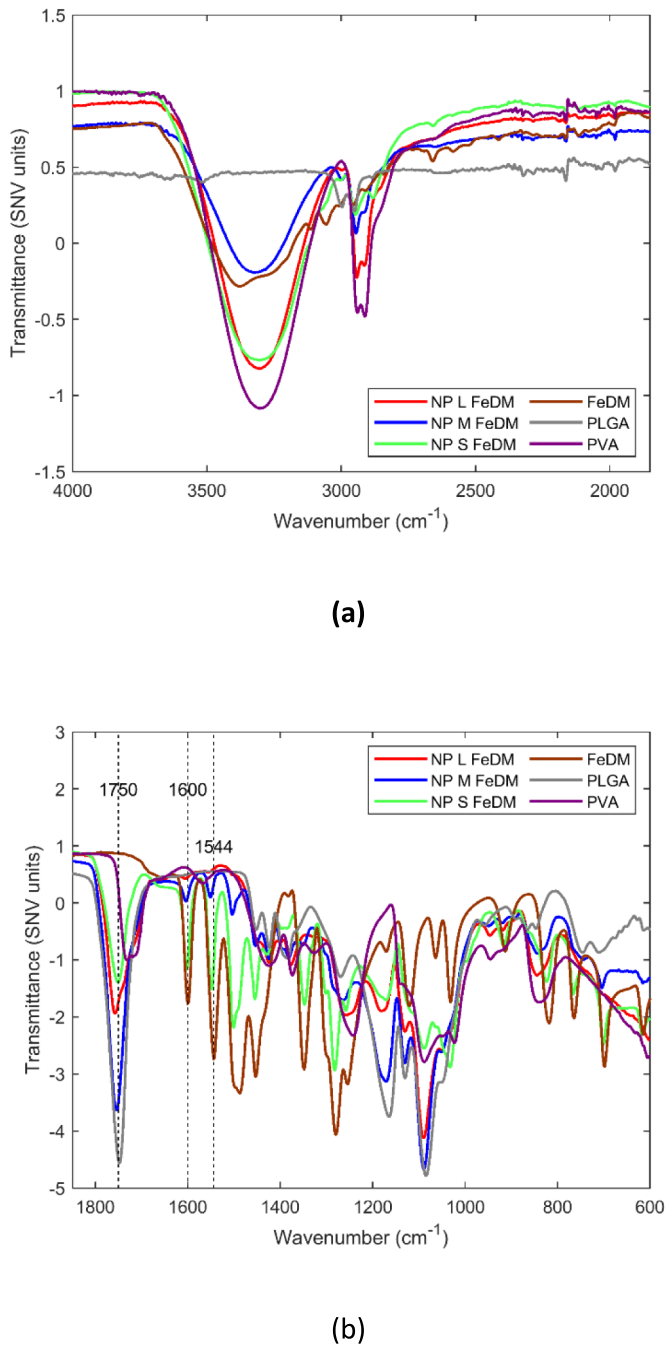

Fig. 4 Fourier-transform infrared spectroscopy spectra of the three types (L-large; M-medium; S-small) of FeDM-loaded NPs, FeDM, Poly(D,L-lactide-co-glycolide) (PLGA) and Poly(vinyl alcohol) (PVA), from 4000 to 1850 cm^{-1} **(a)** and from 1849 to 600 $cm.^{-1}$ **(b)**

FeDM-loaded nanoparticles' storability

The next stage of the study consisted of analysing the storage stability of FeDM-NPs, in order to determine the variation of the physicochemical properties along the time. The results are demonstrated in Figures A.2-A.4 of the ESI.

The "small" FeDM-NPs (Figure A.2) kept at 4 ºC had all their physicochemical properties remain stable over the full duration of the study, while the ones kept

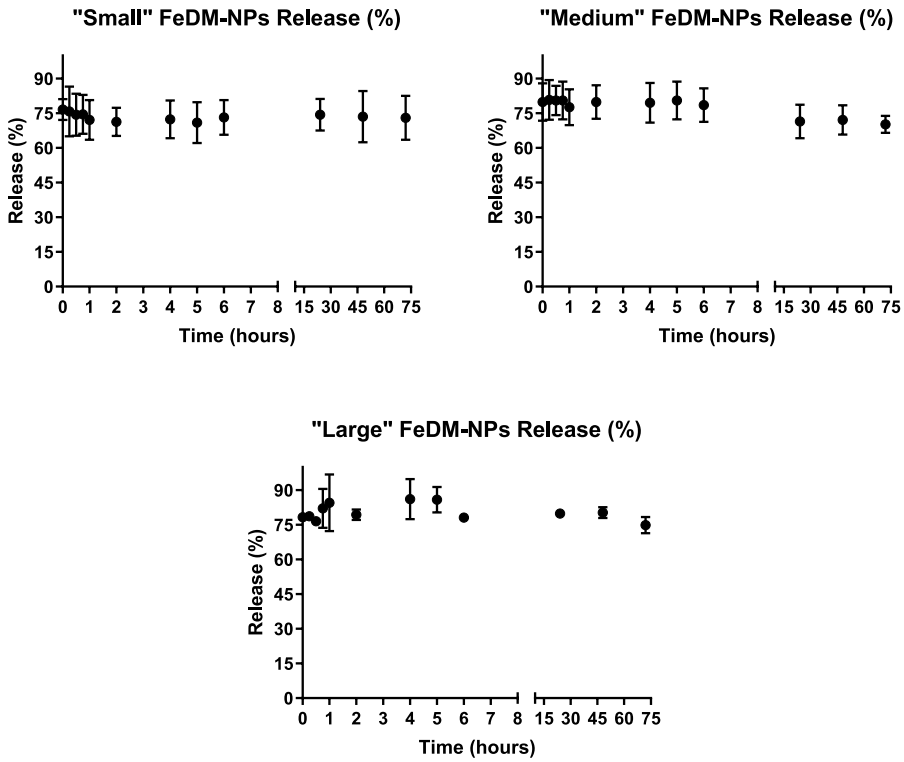

Fig. 5 Release study for "small" (**a**), "medium" (**b**) and "large" (**c**) FeDM-NPs. No significant differences ($p > 0.05$) were found between any point and the 0 h point

at room temperature had their PDI significantly ($p < 0.01$) increased in week 6 compared to week 0.

Regarding the "medium" FeDM-NPs (Figure A.3), all properties remained stable for both temperature groups up to week 2. At week 4 and up to week 6, the zeta potential for both groups increased significantly ($p < 0.0001$) compared to the value recorded in week 0 for each respective group. Throughout the study period, no significant differences ($p > 0.05$) were observed between the two temperature groups.

Concerning the "large" FeDM-NPs (Figure A.4), their size, PDI and zeta potential remained ($p > 0.05$) stable through the six weeks of the study, as well as between the two temperatures. Regarding EE and LC, both groups had a significant ($p < 0.01$) increase in week 1, and these values remained relatively stable until week 6, being higher than week 0 at all points with different degrees of confidence. In the final week, the two properties were still significantly ($p < 0.001$) higher for the particles kept at room temperature compared to week 0, and even higher ($p < 0.0001$) for the ones kept at 4ºC. The values remained equal between conditions over the weeks except in the last week, where the EE and LC of the NSs kept at 4 ºC were significantly ($p < 0.01$) higher than those that were kept at room temperature.

Effect of FeDM-loaded nanoparticles in soybean plants

Morpho-physiological analysis

Soybean seeds were treated with different concentrations of "medium" NSs, chosen due to their more favourable morphological and release properties, as well as being more easily taken up by the plant, as revealed by the RB study, and solutions, and grown under alkaline conditions, to test the efficacy of the NPs in reducing the symptoms of IDC Fig. 6.

Several parameters were analysed for each group of plants. These included physiological parameters such as the time it took from sowing to reach each developmental stage, plant height, and the SPAD values at stages V1 to V3, along with root and shoot fresh weights on the final day of the study.

Regarding the number of days necessary to reach each developmental stage (Fig. 7), it was observed

that all groups achieved the emergence stage and V2 (two fully expanded trifoliate leaves) concurrently. However, only the group exposed to 20 µM "medium" FeDM NSs attained stage V1 in fewer days (12.67 ±1.21) compared to the control (15.17 ±1.47) ($p < 0.05$). Additionally, this group, along with the one treated with a 20 µM solution, progressed to stage V3 more rapidly (20.50 ±1.05 and 20.50 ±1.38, respectively) than the control group (23.33 ±3.34) ($p < 0.05$).

Relating to SPAD values (Fig. 8), only the groups exposed to NSs demonstrated statistically higher SPAD levels compared to the control at stage V1 ($p < 0.05$), although these levels were not significantly different from those in groups treated with FeDM solutions. At the V2 stage both 10 µM and 20 µM FeDM NSs, as well as the 20 µM FeDM solution-treated group showed SPAD levels significantly above the control ($p < 0.05$). At the V3 stage, all FeDM solution and NS-treated groups exhibited higher SPAD values than the control, notably with the 20 µM solution and NS treatments yielding significantly greater values than the 10 µM solution treatment ($p < 0.05$).

Regarding the fresh weights of roots and shoots (Fig. 9), both reveal that plants treated with 20 µM NSs had significantly more ($p < 0.05$) weight than control and plants treated with 10 µM solutions and NSs. However, there were no substantial differences between plants treated with 20 µM NS and the solution of the same concentration.

Genetic expression evaluation

The study also involved investigating the expression patterns of iron metabolism-related genes, including *ferritin*, *FRO2*, and *IRT1* (Fig. 10). No significant differences were detected in the relative gene expression of root *FRO2* in any treatment. Regarding root *IRT1* however, the group of plants treated with 20 µM NSs was the only one having a significantly higher expression (2.25-fold) compared to control. Concerning the relative expression of leaf *ferritin,* both groups treated with NSs

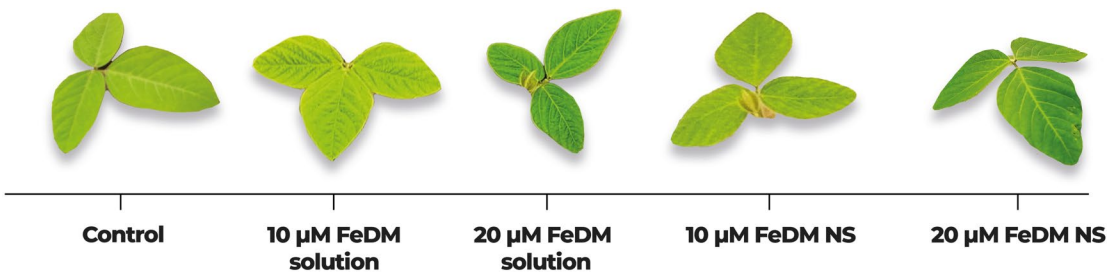

Fig. 6 Trifoliate leaves of plants at the V3 phenological stage, either untreated (control) or treated with 10 µM or 20 µM FeDM solution, or 10 µM or 20 µM FeDM NS

Fig. 7 Number of days required to reach each developmental stage after sowing the seeds, for each treatment. Different letters in each developmental stage indicate significant differences ($p < 0.05$) by two-way ANOVA with Tukey's test

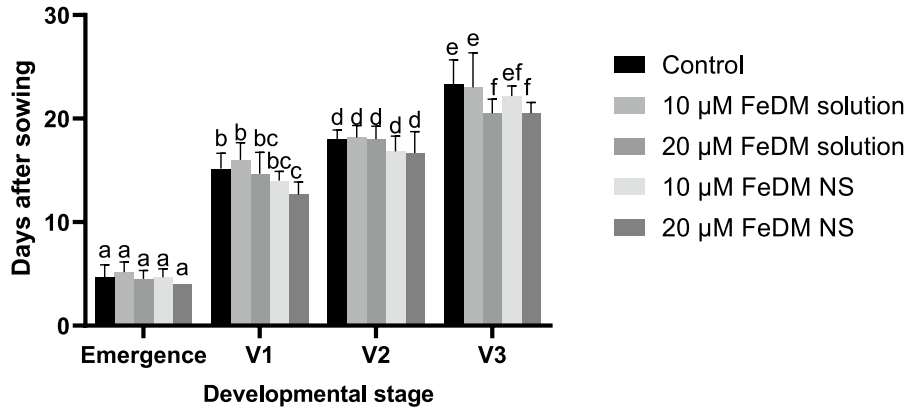

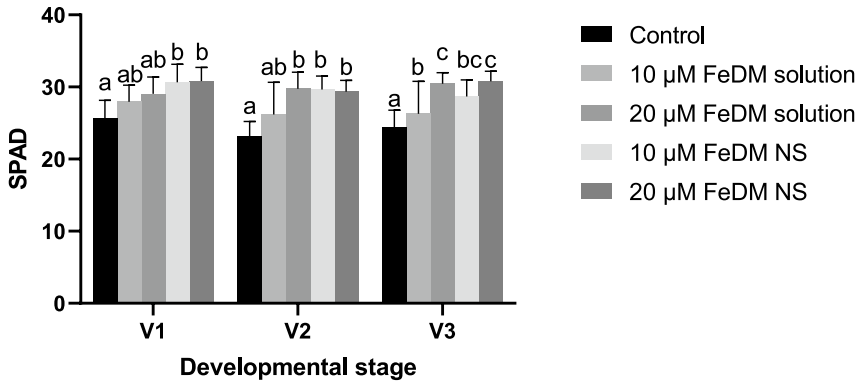

Fig. 8 Soil Plant Analysis Development (SPAD) values per treatment. Different letters in each developmental stage indicate significant differences ($p < 0.05$) by two-way ANOVA with Tukey's test

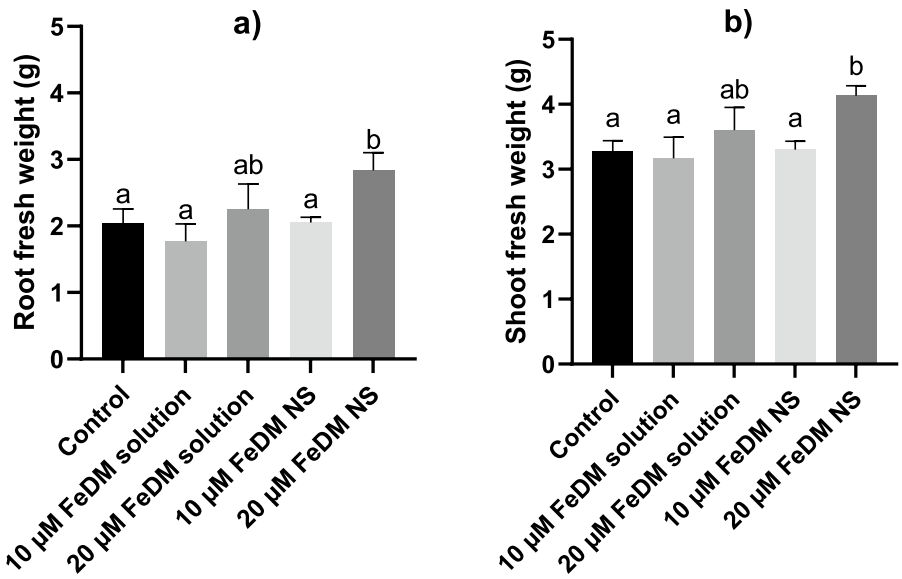

Fig. 9 Fresh weight of roots (**a**) and shoots (**b**), in grams. Different letters indicate significant differences ($p < 0.05$) by one-way ANOVA with Fisher's Uncorrected LSD method

had significantly higher expressions than those of control and treated with 10 µM solution.

Structural analysis of plants' leaves by FTIR and PLSDA

This study aimed to get insight on eventual structural changes caused by FeDM treatments on plants' leaves at V3 stage.

Among the evaluated spectral regions and preprocessing methods, the second spectral region (R2) pre-processed with Savitzky-Golay filtering (15 points, second-order polynomial, second derivative) and a LV exhibited the best performance, correctly classifying 84.61% of the samples. The confusion matrix (Table 3) summarizes the classification for each class.

While classes 1 and 3 were perfectly classified, a 15.38% misclassification rate was observed for class 2 samples, which were sometimes incorrectly categorized as class 1.

Discussion

The main objective of the present work was to produce nanofertilisers able to provide iron to soybean plants and assess how well they can be absorbed and

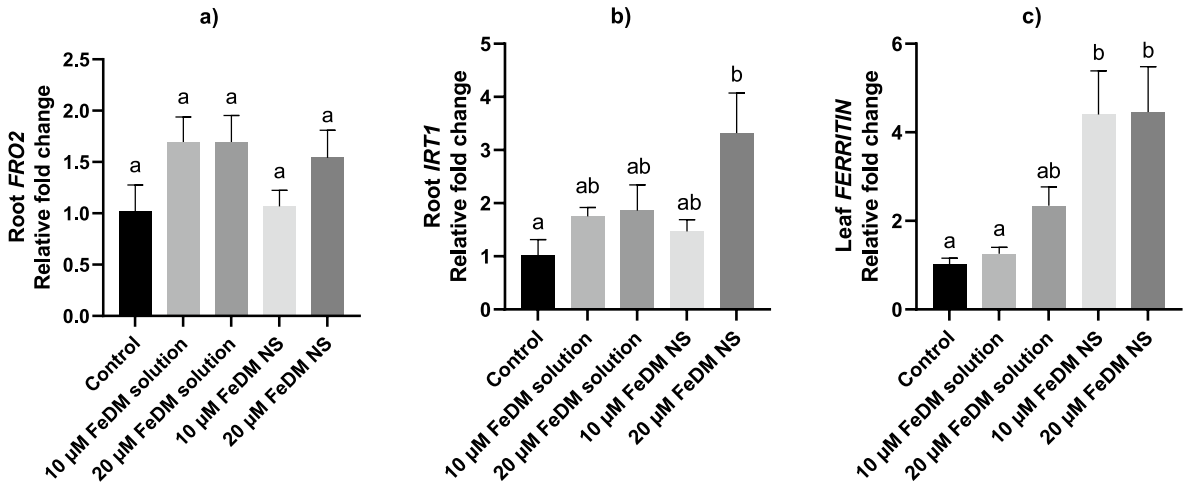

Fig. 10 Relative gene expression of root *FRO2* (**a**) and *IRT1* (**b**), and leaf *ferritin* (**c**), per treatment. Different letters indicate significant differences ($p < 0.05$) by two-way ANOVA with Šidák's test

Table 3 Confusion matrix for the correct prediction for the three classes: Class 1-control; Class 2-FeDM solution; Class 3-FeDM NS

	Class 1	Class 2	Class 3
Class 1	7.69	15.38	0.00
Class 2	0.00	30.77	0.00
Class 3	0.00	0.00	46.15

metabolized compared to regular fertiliser solutions. In order to get insight on the relevance of NPs' size for their uptake by plants, several fluorescent-labelled polymeric NSs were produced to obtain NPs with a range of size. This may be a key step in ascertaining the efficiency with which plant tissues could absorb these particles and then manage IDC. Polydispersity index (PDI), which is associated with the degree of homogeneity of the NPs, is usually considered acceptable in the range of 0.3 and below, since the particles are intended for fertiliser delivery (Zhang and Wang 2023). Additionally, particles with negative zeta-potentials are more likely to be translocated into the apoplast (Lv et al. 2019); and with substantial EE and LC compounds are more successfully incorporated into the polymeric matrix, ensuring that the NPs are able to carry them to the desired location (Giridhar Reddy and Thakur 2019; Massella et al. 2018). For these reasons, the three previously described groups of NPs were chosen to proceed to further characterization.

The data relating to the unloaded NPs and their comparison to the one regarding the RB-NPs (Table 1) shows that the presence of RB does not change the physicochemical properties of the "small" and "large" RB-NPs, while the "medium" RB-NPs were shown to be significantly larger when encapsulating the compounds. This fact can be an indication of the successful incorporation of RB into the polymeric matrix of the NPs (Stenzel 2021).

Through the spectra of RB-loaded NPs and their respective reagents (Fig. 2) we concluded that "medium" and "large" RB-NPs appear to have the same key chemical bonds as PVA at 3310 cm^{-1}, showing that this surfactant is a part of the structure of the particles. We can observe the peak at 1749 cm^{-1} of PLGA in all the particles, due to it being the main component in the polymeric matrix. The peaks at 1644, 1588, and 1338 cm^{-1} seen in RB are present in the "small" RB-loaded NPs, due since these have a concentration of 2% (v/v) of this compound, while the "medium" ones have 1% (v/v) and the "large" ones have 1.5% (v/v). Overall, the results confirmed the successful incorporation of the different components in the obtained formulations.

From FigureA.1, it can be concluded that, all three types of NPs were able to retain the initial amount of compound encapsulated over three days, with no

additional release to the medium. These results show that all three NSs have the potential to act as a reservoir of the compound for that time, which is a positive characteristic, since it means that the NPs can remain in contact with the target tissues for at least three days and keep a percentage of compound available for plants utilization.

The uptake of the different RB-NPs and free RB by the plants was evaluated by measuring RB fluorescence in the roots, stems and leaves using confocal microscopy. As shown in Figs. 2 and 3, no fluorescent signal was detected in the control groups, confirming that all observed fluorescence in the treatment groups was due to RB. For the roots, all three types of NPs were internalized more effectively than the RB solution, a fact that can be explained by the better uptake ability of the compound when entrapped in a polymeric matrix, in this case of PLGA. Treatment with "medium" and "large" RB-NPs resulted in a significantly higher fluorescent signal compared to "small" NPs, suggesting greater internalization of these NP types by the plant roots. Concerning the stems, "medium" RB-NPs treatment induced a significantly higher fluorescent signal than the free RB solution and both "small" and "large" RB-NPs, which supports the data obtained for the roots, indicating a higher internalization and ability of "medium" RB-NPs to reach the stem. Similarly, in the leaves, significant differences were observed between "medium" RB-NPs in comparison to both "small" and "large" RB-NPs. Additionally, "medium" NPs were the only treatment to show a significantly higher uptake compared to the control group. Overall, these findings suggest that "medium" NPs were more effectively internalized than the other NPs and the free RB solution, enabling them to reach the plant leaves.

The results concerning the physicochemical characterization of the FeDM-NPs (Fig. 3) revealed that all the designed formulation have the adequate characteristics to be assessed as nanofertilisers, since the size values are comprised from approximately 100 to 300 nm and the zeta potential values are negative. The obtained values for EE and LC are satisfactory for the purpose since the previously established effective concentration of 10–20 μM (Santos et al. 2020) of compound were ensured in all prepared NSs.

Based on the FTIR data for the FeDM-NPs and their corresponding reagents (Fig. 4), it is possible to conclude that chemical bonds found in PLGA (1750 cm^{-1}) are present in all NPs, showing that a polymeric matrix is found in all of them. Additionally, signals found in PVA (3310 cm^{-1}) are found in the spectra of NPs that use that surfactant. Moreover, characteristic peaks seen in FeDM at 1600 cm^{-1} and 1544 cm^{-1} are seen in FeDM-NPs. It can therefore be concluded that the NPs were successful in encapsulating the iron chelate.

Regarding the stability studies of the FeDM-NPs, the "small" ones (Figure A.2), are more stable when stored at 4ºC. Concerning the "medium" NPs (Figure A.3), their surface charge increases from week two onward, and there is no difference in the temperature they are stored at. Lastly, the "large" FeDM-NPs (Figure A.4) are better kept at 4ºC since they have better encapsulation properties.

Considering all the characterization data and the results from the uptake of fluorescent labelled-NPs, the "medium" FeDM-NPs were chosen to proceed with the in vivo studies in soybean plants.

In Fig. 7, the groups treated with the 20 μM FeDM solution and 20 μM FeDM-NPs advanced from stage V2 to V3 more rapidly than the other groups. This accelerated growth enhances productivity and supports quicker resilience to IDC stress. Also, the groups treated with NSs consistently had higher SPAD values than the control across all developmental stages (Fig. 8) and the 10 μM also recorded a higher level than its solution counterpart, suggesting that at this concentration, NS treatments might be more effective than the respective chelates' solutions. As demonstrated by previous studies (Ferreira et al. 2019; Kobraee 2016; Li et al. 2021), SPAD levels are related to iron, since this mineral is essential for chlorophyll synthesis, which allows the entire system to function properly, as opposed to in iron deficient conditions. These results indicate that the iron present in the NPs was successfully absorbed by plants and transported into the leaves, becoming bioavailable for the synthesis of chlorophyll. Accordingly, 20 μM FeDM NS was the only treatment that showed significantly higher biomass than the control group (Fig. 9). Previous research comparing dry weights of hydroponically grown plants treated with FeDM with plants grown in iron-deficient conditions showed that roots of plants treated with the compound were significantly heavier than those in iron deficiency, however, the weight of the shoots was not significantly higher than control (Santos et al. 2021). The results for 20

μM solution treatment in the shoots compared to the iron-deficient plants are similar to the ones in this study, since the weight of the treated plants' shoots is not significantly different. This result reinforces that the 20 μM NS was more effective in reducing the symptoms of IDC in shoots since it was the only treatment that made the exposed plants' roots heavier than control. Since an adequate amount of bioavailable iron has been shown to increase biomass, this fact suggests that the 20 μM FeDM-NPs were able to provide an appropriate level of iron to the plants (Rotaru and Gusan 2021). A study using iron oxide NPs applied to the leaves of soybean plants obtained similar results, significantly increasing fresh weights (Cao et al. 2022). Since iron deficiency chlorosis has been shown to reduce soybean plants' biomass, these NPs might be a valuable asset in managing a condition (Bai et al. 2018).

To further understand the efficacy of the developed NPs, a genetic expression study was conducted (Fig. 10), with the intent of obtaining information on the levels of expression of three key genes associated with iron storage, transport and absorption: *ferritin*, a gene responsible the production of a protein that stores iron in the leaves, which is regulated primarily by the presence of this element (Masuda et al. 2001); *FRO2,* which encodes ferric reductase, an enzyme responsible for reducing iron in the soils to a more water-soluble form, and requires the presence of iron for its expression; and *IRT1*, which encodes an iron transporter protein, allowing for the mobility of iron inside the roots, and has also been shown to be induced by the presence of this element near root cells (Roriz et al. 2021; Vert et al. 2003). While *FRO2* expression showed no significant differences among treatments, the expression of the *IRT1* gene (Fig. 10 (b)) was increased in the group of plants treated with the 20 μM NSs when compared to the control. The genes encoding *IRT1* and *FRO2* have been shown to be upregulated in conditions of iron deficiency, since the production of these proteins continues for as long as the plant is exposed to iron stress, in order to try to scavenge the uptake of this element (Santos et al. 2020). As said previously, studies have also shown that *IRT1* is induced by the presence of iron in the vicinity of root cells (Vert et al. 2003). This suggests that, at this concentration, the NPs were able to provide iron in a bioavailable form to induce the expression of this gene, further revealing their potential as iron nanofertilisers.

Conversely, ferritin protein expression is low in Fe-deficient plants, since the production of this protein is correlated with the accumulated amount of iron (Kanobe et al. 2013). Here, both groups treated with NSs had higher expressions than those of control and treated with 10 μM solution, potentially showing that even at the 10 μM concentration, NPs were more efficient in delivering iron to the leaves than the solution. This suggests that this product has a potential to be more effective in delivering bioavailable iron to soybean plants than the application via iron chelate solutions. The plants treated with the 20 μM NS were also, on average very successful at delivering iron up the plant – since it is well established that leaf *ferritin* is upregulated in the presence of iron in leaves (Goto et al. 1998). These results further corroborate that these NPs were able to deliver iron to soybean plants, with their effectiveness at the concentration of 10 μM being higher than the solution of the same concentration.

FTIR analysis revealed that FeDM NPs induced detectable structural changes in the plants, likely due to nanoparticle-tissue interactions. PLSDA successfully distinguished control plants from those treated with FeDM NPs with 100% accuracy, indicating significant alterations in molecular composition. However, plants treated with FeDM solutions were not completely distinguishable from the controls, suggesting less effective structural changes with solution-based delivery (Table 3).

To sum up, the use of Fe-chelate-loaded NPs had a positive effect on soybean plants grown in iron-deficient, calcareous soils, as evidenced by improvements in chlorophyll content, growth rate, and the fresh weight of roots and shoots. The increase in expression of genes related to iron metabolism such as *ferritin* and *IRT1*, aligned with the observed morphological improvements, suggesting an effect at the molecular level of the NP treatment. These findings evidence a strong potential for these NPs as an alternative to traditional iron fertilisers, offering a new solution to combat IDC in crops.

Due to the long persistence of certain agrochemicals on the soil, as well as their contamination of groundwaters, it is imperative to develop new delivery methods to minimize such impact. Sustainable agriculture is essential to achieve the United Nation's Agenda 2030, and these NPs can be an advantageous tool to achieve sustainability, potentially reducing

fertiliser leachate and maintaining a more sustained release. The encapsulation properties of the NPs, as well as their effectiveness in reducing chlorosis symptoms, makes these formulations promising, and demonstrates how nanotechnology can be used to improve agricultural yields and reduce agrochemical waste.

Therefore, it is important to thoroughly study the persistence and biodegradability of PLGA in soils, to guarantee its safety as a nanocarrier, as well other application methods such as foliar and soil application. Furthermore, this formulation should also be attempted with other Fe-chelates and other chelated ions, to address other mineral shortages in plants.

Acknowledgements This work received financial support from the PT national funds (FCT/MCTES, Fundação para a Ciência e Tecnologia and Ministério da Ciência, Tecnologia e Ensino Superior) through the projects UID/50006 -Laboratório Associado para a Química Verde - Tecnologias e Processos Limpos, UIDB/50016/2020 (DOI 10.54499/UIDB/50016/2020), UIDB/50006/2020 (DOI 10.54499/UIDB/50006/2020), UIDP/50006/2020 (DOI 10.54499/UIDP/50006/2020), and LA/P/0008/2020 (DOI 10.54499/LA/P/0008/2020). C. Santos and M. Sarraguça thank FCT for funding through the Individual Call to Scientific Employment Stimulus grants 2022.01903.CEECIND (10.54499/2022.01903.CEECIND/CP1745/CT0002) and 2022.01388.CEECIND/CP1724/CT0003 (10.54499/2022.01388.CEECIND/CP1724/CT0003), respectively.

Author contributions S. Pinho: Investigation, Formal analysis, Writing—Original Draft, Writing—Review & Editing. C. Santos: Supervision, Conceptualization, Writing—Review & Editing. T. Moniz: Supervision, Conceptualization, Funding acquisition, Resources, Writing—Review & Editing. A. Granja: Investigation, Writing—Review & Editing, Formal analysis. M. Sarraguça: Investigation, Writing—Review & Editing, Formal analysis. S. Reis: Supervision, Funding acquisition, Resources, Writing—Review & Editing. M. Rangel: Supervision, Funding acquisition, Resources, Writing—Review & Editing. M. Vasconcelos: Supervision, Funding acquisition, Resources, Writing—Review & Editing.

Funding Open access funding provided by FCT|FCCN (b-on). This work received financial support from PT national funds (FCT/MCTES, Fundação para a Ciência e Tecnologia and Ministério da Ciência, Tecnologia e Ensino Superior) through the projects EXPL/QUI-QIN/0411/2021, LA/P/0008/2020, UIDB/50006/2020 and UIDP/50006/2020.

Data Availability The data are available from the corresponding author on request.

Declarations

Conflicts of interest The authors declare no conflict of interest.

Open Access This article is licensed under a Creative Commons Attribution 4.0 International License, which permits use, sharing, adaptation, distribution and reproduction in any medium or format, as long as you give appropriate credit to the original author(s) and the source, provide a link to the Creative Commons licence, and indicate if changes were made. The images or other third party material in this article are included in the article's Creative Commons licence, unless indicated otherwise in a credit line to the material. If material is not included in the article's Creative Commons licence and your intended use is not permitted by statutory regulation or exceeds the permitted use, you will need to obtain permission directly from the copyright holder. To view a copy of this licence, visit http://creativecommons.org/licenses/by/4.0/.

References

Bai G, Jenkins S, Yuan W, Graef GL, Ge Y (2018) Field-Based scoring of soybean iron deficiency chlorosis using RGB imaging and statistical learning. Front Plant Sci 9:1002. https://doi.org/10.3389/fpls.2018.01002

Bukhari A, Fatima Z, Atta M, Nazir A, Alshawwa SZ, Alotaibi HF, Iqbal M (2023) Poly lactic-Co-glycolic acid nanocarriers for encapsulation and controlled release of hydrophobic drug to enhance the bioavailability and antimicrobial properties. Dose Response 21:15593258231152116. https://doi.org/10.1177/15593258231152117

Cao X, Yue L, Wang C, Luo X, Zhang C, Zhao X, Wu F, White JC, Wang Z, Xing B (2022) Foliar application with iron oxide nanomaterials stimulate nitrogen fixation, yield, and nutritional quality of soybean. ACS Nano 16:1170–1181. https://doi.org/10.1021/acsnano.1c08977

Carvalho SMP, Vasconcelos MW (2013) Producing more with less: strategies and novel technologies for plant-based food biofortification. Food Res Int 54:961–971. https://doi.org/10.1016/j.foodres.2012.12.021

Chang J, Jallouli Y, Kroubi M, Yuan X-B, Feng W, Kang C-S, Pu P-Y, Betbeder D (2009) Characterization of endocytosis of transferrin-coated PLGA nanoparticles by the blood–brain barrier. Int J Pharm 379:285–292. https://doi.org/10.1016/j.ijpharm.2009.04.035

Chaves LL, Costa Lima SA, Vieira ACC, Barreiros L, Segundo MA, Ferreira D, Sarmento B, Reis S (2018) Development of PLGA nanoparticles loaded with clofazimine for oral delivery: assessment of formulation variables and intestinal permeability. Eur J Pharm Sci 112:28–37. https://doi.org/10.1016/j.ejps.2017.11.004

Ferreira CMH, Lopez-Rayo S, Lucena JJ, Soares EV, Soares H (2019) Evaluation of the efficacy of two new biotechnological-based freeze-dried fertilizers for sustainable fe deficiency correction of soybean plants grown in calcareous soils. Front Plant Sci 10:1335. https://doi.org/10.3389/fpls.2019.01335

Fonseca M, Macedo AS, Lima SAC, Reis S, Soares R, Fonte P (2021) Evaluation of the antitumour and antiproliferative effect of xanthohumol-loaded PLGA nanoparticles on melanoma. Materials (Basel) 14:6422. https://doi.org/10.3390/ma14216421

Giridhar Reddy S, Thakur A (2019) Drug Entrapment Efficiency of Silver Nanocomposite Hydrogel. IOP Conference Series: Mater Sci Eng 577. https://doi.org/10.1088/1757-899x/577/1/012176.

Goto F, Yoshihara T, Saiki H (1998) Iron accumulation in tobacco plants expressing soyabean ferritin gene. Transgenic Res 7:173–180. https://doi.org/10.1023/a:1008836812714

Hua Y, Su Y, Zhang H, Liu N, Wang Z, Gao X, Gao J, Zheng A (2021) Poly(lactic-co-glycolic acid) microsphere production based on quality by design: a review. Drug Deliv 28:1342–1355. https://doi.org/10.1080/10717544.2021.1943056

Kanobe MN, Rodermel SR, Bailey T, Scott MP (2013) Changes in endogenous gene transcript and protein levels in maize plants expressing the soybean ferritin transgene. Front Plant Sci 4:196. https://doi.org/10.3389/fpls.2013.00196

Kharazmi A, Faraji N, Mat Hussin R, Saion E, Yunus WM, Behzad K (2015) Structural, optical, opto-thermal and thermal properties of ZnS-PVA nanofluids synthesized through a radiolytic approach. Beilstein J Nanotechnol 6:529–536. https://doi.org/10.3762/bjnano.6.55

Khodakovskaya M, Marmiroli M (2023) Editorial: Polymeric nanoparticles for sustainable plant agriculture and food industry. Front Plant Sci 14:1183938. https://doi.org/10.3389/fpls.2023.1183938

Kobayashi T, Nishizawa NK (2012) Iron uptake, translocation, and regulation in higher plants. Annu Rev Plant Biol 63:131–152. https://doi.org/10.1146/annurev-arplant-042811-105522

Kobraee S (2016) Effect of zinc, iron and manganese fertilization on concentrations of these metals in the stem and leaves of soybean and on the chlorophyll content in leaves during the reproductive development stages. J Elementol 21:395–412. https://doi.org/10.5601/jelem.2015.20.2.966

Li J, Cao X, Jia X, Liu L, Cao H, Qin W, Li M (2021) Iron deficiency leads to chlorosis through impacting chlorophyll synthesis and nitrogen metabolism in areca catechu L. Front Plant Sci 12:710093. https://doi.org/10.3389/fpls.2021.710093

Livak KJ, Schmittgen TD (2001) Analysis of relative gene expression data using real-time quantitative PCR and the 2(-Delta Delta C(T)) Method. Methods 25:402–408. https://doi.org/10.1006/meth.2001.1262

Lucena JJ, Hernandez-Apaolaza L (2017) Iron nutrition in plants: an overview. Plant Soil 418:1–4. https://doi.org/10.1007/s11104-017-3316-8

Lv J, Christie P, Zhang S (2019) Uptake, translocation, and transformation of metal-based nanoparticles in plants: recent advances and methodological challenges. Environ Sci: Nano J 6:41–59. https://doi.org/10.1039/c8en00645h

Marschner H, Römheld V (1994) Strategies of plants for acquisition of iron. Plant Soil 165:261–274. https://doi.org/10.1007/bf00008069

Massella D, Celasco E, Salaun F, Ferri A, Barresi AA (2018) Overcoming the Limits of Flash Nanoprecipitation: Effective Loading of Hydrophilic Drug into Polymeric Nanoparticles with Controlled Structure. Polymers (Basel) 10. https://doi.org/10.3390/polym10101092.

Mastronardi ET, Phepafatso & Zhang, Xueru & Monreal, Carlos & Derosa, Maria (2015) Strategic Role of Nanotechnology in Fertilizers: Potential and Limitations. Nanotechnologies in Food and Agriculture: 46. https://doi.org/10.1007/978-3-319-14024-7_2

Masuda T, Goto F, Yoshihara T (2001) A novel plant ferritin subunit from soybean that is related to a mechanism in iron release. J Biol Chem 276:19575–19579. https://doi.org/10.1074/jbc.M011399200

Merry R, Espina MJ, Lorenz AJ, Stupar RM (2022) Development of a controlled-environment assay to induce iron deficiency chlorosis in soybean by adjusting calcium carbonates, pH, and nodulation. Plant Methods 18:36. https://doi.org/10.1186/s13007-022-00855-5

Mesquita LS, Mesquita RBR, Leite A, Moniz T, Rangel M, Rangel AOSS (2020) Integrated flow-based system displaying an in-line mini soil column to monitor iron species in soils leachates. Commun Soil Sci Plant Anal 51:1089–1100. https://doi.org/10.1080/00103624.2020.1751186

Mesquita RBR, Moniz T, Nunes MJM, Mesquita LS, Rangel M, Rangel A (2022) Sequential injection method for biparametric determination of iron and manganese in soil leachates. Anal Methods 14:180–187. https://doi.org/10.1039/d1ay01932e

Mittal D, Kaur G, Singh P, Yadav K, Ali SA (2020) Nanoparticle-based sustainable agriculture and food science: recent advances and future outlook. Front Nanotechnol 2:1–38. https://doi.org/10.3389/fnano.2020.579954

Morrissey J, Guerinot ML (2009) Iron uptake and transport in plants: the good, the bad, and the ionome. Chem Rev 109:4553–4567. https://doi.org/10.1021/cr900112r

OECD (1984) Earthworm, Acute Toxicity Tests. OECD Guidelines for the Testing of Chemicals. https://doi.org/10.1787/9789264070042-en

Peiffer GA, King KE, Severin AJ, May GD, Cianzio SR, Lin SF, Lauter NC, Shoemaker RC (2012) Identification of candidate genes underlying an iron efficiency quantitative trait locus in soybean. Plant Physiol 158:1745–1754. https://doi.org/10.1104/pp.111.189860

Queiros C, Amorim MJ, Leite A, Ferreira M, Gameiro P, de Castro B, Biernacki K, Magalhães A, Burgess J, Rangel M (2011) Nickel(II) and Cobalt(II) 3-Hydroxy-4-pyridinone Complexes: Synthesis, Characterization and Speciation Studies in Aqueous Solution. European J Inorg Chem 131–140. https://doi.org/10.1002/ejic.201000849

Roriz M, Pereira SIA, Castro PML, Carvalho SMP, Vasconcelos MW (2021) Iron metabolism in soybean grown in calcareous soil is influenced by plant growth-promoting rhizobacteria – A functional analysis. Rhizosphere 17:1–7. https://doi.org/10.1016/j.rhisph.2020.100274

Rotaru V, Gusan A (2021) Effects of phosphorus and iron on biomass production and nutrients partitioning in soybean cultivars under water stress condition. World J Adv Res Rev 12:414–422. https://doi.org/10.30574/wjarr.2021.12.3.0686

Rout GR, Sahoo S (2015) Role of iron in plant growth and metabolism. Rev Agric Sci 3:1–24. https://doi.org/10.7831/ras.3.1

Santos CS, Carvalho SM, Leite A, Moniz T, Roriz M, Rangel AO, Rangel M, Vasconcelos MW (2016a) Effect of

tris(3-hydroxy-4-pyridinonate) iron(III) complexes on iron uptake and storage in soybean (Glycine max L.). Plant Physiol Biochem 106:91–100. https://doi.org/10.1016/j.plaphy.2016.04.050

Santos CS, Leite A, Vinhas S, Ferreira S, Moniz T, Vasconcelos MW, Rangel M (2020) A combined physiological and biophysical approach to understand the ligand-dependent efficiency of 3-hydroxy-4-pyridinone Fe-chelates. Plant Direct 4:e00256. https://doi.org/10.1002/pld3.256

Santos CS, Rodrigues E, Ferreira S, Moniz T, Leite A, Carvalho SMP, Vasconcelos MW, Rangel M (2021) Foliar application of 3-hydroxy-4-pyridinone Fe-chelate [Fe(mpp)(3)] induces responses at the root level amending iron deficiency chlorosis in soybean. Physiol Plant 173:235–245. https://doi.org/10.1111/ppl.13367

Santos CS, Serrão I, Vasconcelos MW (2016b) Comparative analysis of iron deficiency chlorosis responses in soybean (Glycine max) and barrel medic (Medicago truncatula). Revista de Ciências Agrárias 39:538–549. https://doi.org/10.19084/rca16090

Santos MA, Irto A, Buglyo P, Chaves S (2022) Hydroxypyridinone-Based Metal Chelators towards Ecotoxicity: Remediation and Biological Mechanisms. Molecules 27. https://doi.org/10.3390/molecules27061966

Schlindwein W, Waltham E, Burgess J, Binsted N, Nunes A, Leite A, Rangel M (2006) New lipophilic 3-hydroxy-4-pyridinonate iron(III) complexes: synthesis and EXAFS structural characterisation. Dalton Trans 1313–1321. https://doi.org/10.1039/b509671e.

Shinta YC, Zaman B, Sumiyati S (2021) Citric Acid and EDTA as chelating agents in phytoremediation of heavy metal in polluted soil: a review. IOP Conference Series: Earth Environ Sci 896. https://doi.org/10.1088/1755-1315/896/1/012023

Skrzypczak D, Jarzembowski L, Izydorczyk G, Mikula K, Hoppe V, Mielko KA, Pudelko-Malik N, Mlynarz P, Chojnacka K, Witek-Krowiak A (2021) Hydrogel alginate seed coating as an innovative method for delivering nutrients at the early stages of plant growth. Polymers (Basel) 13:4233. https://doi.org/10.3390/polym13234233

Stenzel MH (2021) The trojan horse goes wild: the effect of drug loading on the behavior of nanoparticles. Angew Chem Int Ed Engl 60:2202–2206. https://doi.org/10.1002/anie.202010934

Vega-Vasquez P, Mosier NS, Irudayaraj J (2020) Nanoscale drug delivery systems: from medicine to agriculture. Front Bioeng Biotechnol 8:79. https://doi.org/10.3389/fbioe.2020.00079

Vert GA, Briat JF, Curie C (2003) Dual regulation of the Arabidopsis high-affinity root iron uptake system by local and long-distance signals. Plant Physiol 132:796–804. https://doi.org/10.1104/pp.102.016089

Ylivainio K (2010) Effects of iron(III)chelates on the solubility of heavy metals in calcareous soils. Environ Pollut 158:3194–3200. https://doi.org/10.1016/j.envpol.2010.07.004

Zhang S, Wang C (2023) Effect of stirring speed on particle dispersion in silica synthesis. Nano-Struct Nano-Objects 35:1–3. https://doi.org/10.1016/j.nanoso.2023.100994

Publisher's Note Springer Nature remains neutral with regard to jurisdictional claims in published maps and institutional affiliations.